

Diversifying beam species through decay and recapture ion trapping: a demonstrative experiment at TITAN-EBIT

E Leistenschneider^{1,2} , R Klawitter^{1,3}, A Lennarz^{1,4},
M Alanssari⁴, J C Bale^{1,2}, B R Barquest¹, U Chowdhury^{1,5,9},
A Finlay^{1,2}, A T Gallant^{1,2}, B Kootte^{1,5}, D Lascar¹,
K G Leach^{1,10}, A J Mayer^{1,6}, D Short^{1,7}, C Andreoiu⁷,
G Gwinner⁵, M E Wieser⁶, J Dilling^{1,2} and A A Kwiatkowski^{1,8}

¹ TRIUMF, 4004 Wesbrook Mall, Vancouver, British Columbia V6T 2A3, Canada

² Department of Physics and Astronomy, University of British Columbia, Vancouver, British Columbia V6T 1Z1, Canada

³ Max-Planck-Institut für Kernphysik, D-69117 Heidelberg, Germany

⁴ Institut für Kernphysik, Westfälische Wilhelms-Universität, D-48149 Münster, Germany

⁵ Department of Physics and Astronomy, University of Manitoba, Winnipeg, Manitoba R3T 2N2, Canada

⁶ Department of Physics and Astronomy, University of Calgary, Calgary, Alberta T2N 1N4, Canada

⁷ Department of Chemistry, Simon Fraser University, Burnaby, British Columbia V5A 1S6, Canada

⁸ Department of Physics and Astronomy, University of Victoria, Victoria, British Columbia V8P 5C2, Canada

E-mail: erichleist@triumf.ca

Received 24 October 2019, revised 16 January 2020

Accepted for publication 22 January 2020

Published 9 March 2020



CrossMark

Abstract

Recapturing the recoiling daughters from radioactive decay can be a simple way to diversify beam availability at rare isotope beam facilities. In the decay and recapture ion trapping (DRIT) technique, a parent species is stored in an ion trap and left to decay, and the daughter ions are recaptured by the trap and

⁹ Present address: Canadian Nuclear Laboratories, Chalk River, Ontario K0J 1J0, Canada.

¹⁰ Present address: Department of Physics, Colorado School of Mines, Golden, CO 80401, United States of America.



Original content from this work may be used under the terms of the [Creative Commons Attribution 4.0 licence](https://creativecommons.org/licenses/by/4.0/). Any further distribution of this work must maintain attribution to the author(s) and the title of the work, journal citation and DOI.

become available for use. We successfully demonstrated the technique using the electron beam ion trap (EBIT) at the TITAN facility. A pure cloud of ^{30}Mg ions was stored in the EBIT for about one half-life and sent to a Penning trap mass spectrometer, which confirmed the production of ^{30}Al daughter ions. Systematic measurements and simulations suggest high recapture efficiencies of the recoil ion and little influence of the recoiling energy in the observed losses. With the secondary beam, we also performed precision mass measurements of the parent $^{30}\text{Mg}^{8+}$ and the daughter $^{30}\text{Al}^{11+}$ ions. Our results agree with the literature and improve its precision. The success of this experiment shows that EBITs can produce high-quality beams through the DRIT technique.

Keywords: radioactive ion beams, ion trapping, mass spectrometry

(Some figures may appear in colour only in the online journal)

1. Introduction

Access to exotic radioactive nuclei enables a broad range of scientific investigations from fundamental to applied sciences. Improving their production techniques by focusing on quality, intensity, purity, efficiency and selectivity, has been a highly active area of research [1]. Generally, most modern techniques produce rare isotope beams (RIBs) through nuclear reactions induced by a driver beam on a target. They differ by the method employed in the isolation of the ion of interest (IoI) and its transport to experiments.

The selection of a specific IoI can be challenging in some circumstances: they may suffer from low production cross-sections; they may need to compete with more abundant co-produced contamination; and, their extraction and selection may be subject to very low efficiencies. For example, in the isotope separation on-line (ISOL) method [1] the RIBs are stopped and thermalized inside the production target. The target is coupled to an ion source and the ionized beam cocktail is sent through a mass separator. The chemical and physical processes that influence the extraction of species of interest from the production target [1, 2], such as ionization potential and volatility, limit the availability of certain beams. Consequently, ion beams of refractory metals and of reactive elements, such as iron and boron, are difficult to produce.

One way to circumvent these limitations in select cases is the decay and recapture ion trapping (DRIT) technique. It consists of storing a cloud of a parent ion in an ion trap for a time comparable to its half-life or longer. Then, a cloud of the IoI can be created if the trapping potential is deep enough to recapture the recoiling products. This allows the production of otherwise inaccessible beams if a RIB facility can provide a parent species. Not only it permits the creation of beams of refractory and reactive elements, in the case of ISOL facilities, but also the creation of isomeric beams.

The technique was first employed at CERN-ISOLDE for the creation of ^{37}Ar [3] and $^{61-63}\text{Fe}$ [4] ions for mass spectrometry experiments. In both cases, parent ions were stored in a buffer-gas-filled Penning trap, which reportedly re-trapped about 50% of recoils. Two other experiments [5, 6] performed in the same facility employed electron beam ion traps (EBIT) [7, 8] as storage device. Evidence from these experiments suggests EBITs are ideal storing devices for this technique.

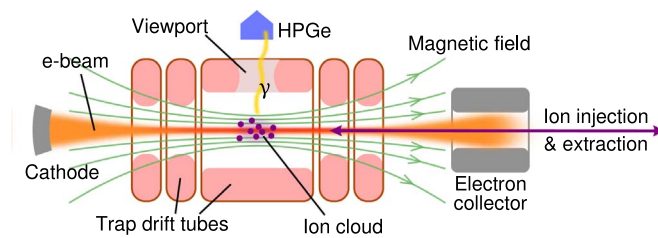


Figure 1. Schematic overview of the TITAN EBIT. Trapping of ions is achieved axially by an electrostatic potential and radially by both a magnetic field and an intense electron beam passing through the trapping region. The γ -rays from radioactive decays are detected by a HPGe detector mounted on a viewport facing the trap interior.

In this work, we further explore the use of such ion traps and report the in-EBIT production of ^{30}Al from a parent beam of ^{30}Mg , performed for the first time at TRIUMF's ion trap for atomic and nuclear science (TITAN) [9]. We characterized the evolution of the trapped contents and adjusted operating parameters to optimize the creation of IoI beam. The ^{30}Al ions were extracted and delivered to another experimental setup—a precision Penning trap mass spectrometer—where their mass was successfully measured.

In the following section, we discuss the technique in detail, as well as the advantages and challenges of using an EBIT as the storage device. In section 3, we present a simple model to describe the evolution of stored radioactive contents in the EBIT, applied to the proof-of-principle experiment herein. In section 4 we provide a description of our apparatus and of the experimental procedures employed. In section 5, we present the results of the systematic investigations on the creation of daughter or secondary beam using the EBIT. In section 6, we demonstrate the production of the secondary beam through unambiguous identification with the mass spectrometer, and describe the subsequent mass measurements performed. We conclude with possible applications of the technique.

2. In-EBIT DRIT

Conceptually the DRIT technique is simple. If a suitable parent species is available, it is stored for the timescale of its half-life and its daughter is recaptured. The key questions lie in the confinement capabilities of the trap: First, can the cloud be stored for such a period? Second, how many of the daughters ions will be retained in the trapping volume? These questions are central to selecting the most suitable trapping setup and, more indirectly, potential candidate species.

Ion traps, such as Penning or Paul traps, typically create potential wells of a few eV to a few keV deep. The three-body β -decay, for example, generates a recoil energy spectrum that spans hundreds of eV. Therefore, β -decay products can be recaptured in typical ion traps. In contrast, α -decays may produce monoenergetic recoils of a few hundred keV, which makes their recapture more challenging. In this article, we focus on the recapture of weak decay products only.

EBITs have storage capabilities that typically outperform other ion traps [7, 8]. They have an electrode structure that provides axial ion confinement overlapped with a strong magnetic field that provides radial confinement. EBITs also have a dense electron beam passing through the trapping region (see figure 1), which ionizes ions through electron impact. For this reason, they are widely used to provide charge-bred beams for experiments or for

post-acceleration [10]. The electron beam greatly deepens confinement; and as the ion's charge state increases, it experiences a deeper trapping potential in all directions. Consequently the recoil energy has less effect on the recapture efficiency. Furthermore, highly charged ions remain charged after decay, whereas singly charged ions may be neutralized in gas-filled traps or following β^+ -decay [3]. Therefore, EBITs offer a nearly ideal environment to recapture decay products.

However, the use of EBITs poses certain challenges: (a) electron-impact ionization generates a distribution of charge states. If the products are transported out of the trap, only a fraction will have the desired charge (typically around 20%) [10, 11]. (b) The electron beam also ionizes residual gases that are present in the trapping volume, which may contaminate the beam. Last (c), EBITs may be 'hot' environments due to complex thermodynamical processes, such as heating of the ion cloud by the electron beam and heat exchange by ion-ion collisions. A large thermal input to the IoI may "boil" them out of the trap, thus reducing the efficiency of the technique.

Therefore, EBIT operating parameters must be carefully tuned in order to balance recapture efficiency, charge breeding, ion-cloud thermodynamics and other physical processes that influence the final quality of the secondary beam. In the next section, we describe the evolution of stored radioactive ions in an EBIT using a simple model, which illustrates some of these challenges and provides a clearer picture of the relevant variables.

3. Simulations of secondary beam creation

To understand the secondary beam creation and its confinement, we simulated the in-trap decay of a cloud of parent ions in the TITAN EBIT, including population evolution and a simple EBIT thermodynamical model. ^{30}Mg was chosen as a suitable parent to explore as a proof-of-principle case, both from its decay properties and from its experimental availability.

The decay chain of $^{30}\text{Mg} \rightarrow ^{30}\text{Al} \rightarrow ^{30}\text{Si}$ provides representative examples of typical β^- decays. First, the half-lives of ^{30}Mg and ^{30}Al , 0.335(10) s [12] and 3.62(6) s [13], respectively, allow us to probe two different timescales of interest, each one order of magnitude apart. Second, the Q_β values of the decays (both above 6 MeV) are higher than average [14], allowing for a higher recoil energy contribution. Their decay schemes are complex, with many intermediate γ de-excitation steps, but well understood [12, 13]. Moreover, $^{30}\text{Mg}^+$ can be provided to TITAN as a pure beam by the ISAC facility. Hence, this decay chain allows a straightforward proof-of-principle experiment to explore the DRIT technique at TITAN.

In a Monte Carlo approach, particles in an initially pure $^{30}\text{Mg}^{q+}$ cloud, where q is the charge state of the ion, were randomly assigned a starting energy following a Maxwell-Boltzmann distribution. Particles were evolved in time (t , iterated by time step Δt) and were subject to three physical processes described below: Spitzer heating, radioactive decay and trap escape. A flow diagram of the employed algorithm is shown in figure 2.

Spitzer heating [7]: Trapped ions constantly gain energy from collisions with the intense electron beam. This is known to be a dominant process in EBIT thermodynamics; if no active cooling mechanism is employed, ions will eventually gain enough energy to escape the trap barriers. The energy input per particle from Spitzer heating is proportional to q^2 and was calculated by the prescription outlined in [7], assuming a perfect overlap between the electron beam and the ion cloud.

Radioactive decay: The population change from decay was modeled through simple decay laws, while heating from the recoil required consideration of the three-body nature of β^- decay. We followed the same kinematic procedure outlined in detail in [4] to calculate the

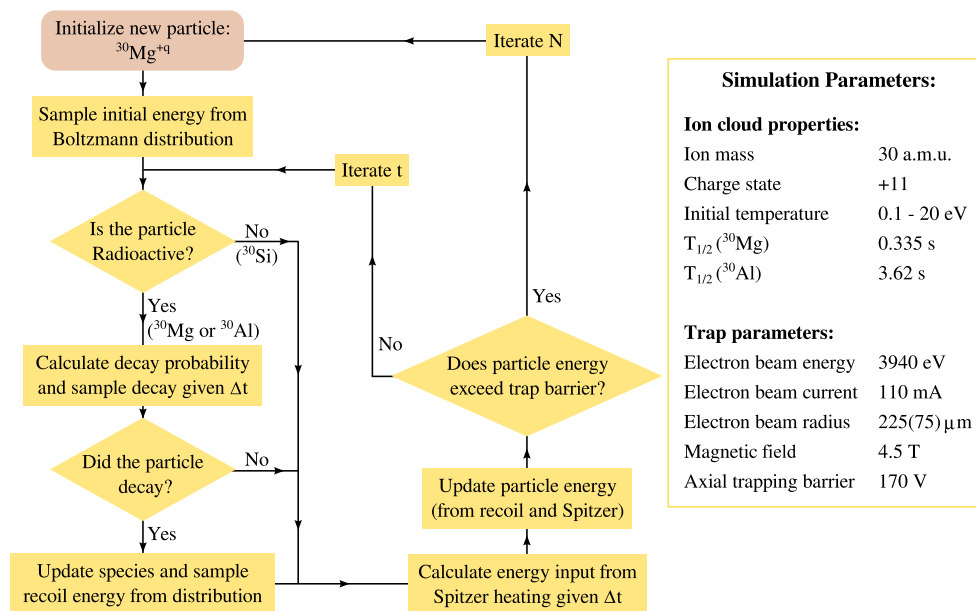


Figure 2. A simplified flow diagram of the Monte Carlo algorithm to calculate secondary beam creation and its confinement in the TITAN EBIT. Only three physical processes are included: Spitzer heating, radioactive decay, and trap escape. The relevant parameters on these processes are described in the table. Nuclear properties were taken from [12, 13], and typical TITAN EBIT operating parameters were chosen.

recoil energy distributions. The calculation included not only the β -decay itself, but also the intermediate de-excitation through γ -emission and all possible known decay branches. The β -decays schemes of ^{30}Mg and ^{30}Al are well described in [12, 13], respectively. These are almost pure Gamow–Teller transitions, for which the spectral shape of recoil energy distribution is well known [15, 16]. In the case of γ -emission, there are no long-lived isomeric states in the cases studied; therefore we assumed that all de-excitations occur instantaneously. The final recoiling energy distributions are shown in figure 3. The Q_{β} -value for ^{30}Al (8561 keV) is higher than that for ^{30}Mg (6990 keV). However, the average recoil energy gained by the daughter in both decays are comparable, 427 eV in the ^{30}Mg decay and 454 eV in the ^{30}Al decay. The ^{30}Al decay mainly decays to much higher excited states of ^{30}Si ; thus in some cases photon emission can revert the orientation of the recoiling momentum gained in the β -decay.

Trap escape: The opportunity to escape from the trap was incorporated at the end of every time step by removing particles from the simulation if their energy exceeded the trapping potential barriers. The escape also cools the trapped ion cloud through evaporative cooling. It was assumed ion losses occur predominantly through axial potential barriers, as prescribed in [7].

For simplicity, other typical EBIT processes [7] such as radiative recombination, charge exchange, ionization heating and effects from ion–ion interaction were neglected. The simulation also did not include the charge-breeding dynamics, and the population was assumed to be in the +11 charge state. The choice of charge state was guided by an EBIT charge-state evolution calculation [7] that showed that the ion cloud should be predominantly

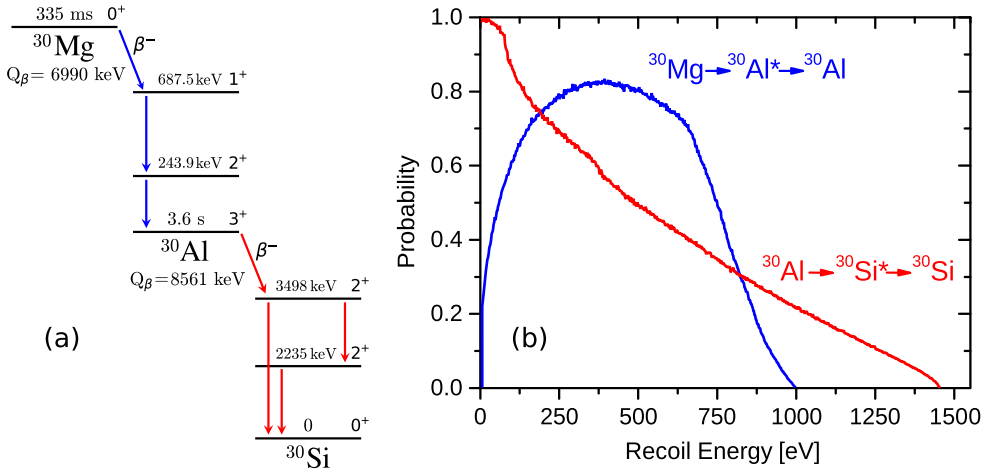


Figure 3. (a) The decay scheme of the $^{30}\text{Mg} \rightarrow ^{30}\text{Al} \rightarrow ^{30}\text{Si}$ chain [12, 13] shows the energy levels and major transitions (arrows). (b) The recoil energy distributions following the β -decays and γ de-excitations of ^{30}Mg and ^{30}Al in the center-of-mass reference frame.

in charge states between +10 and +12 for the timescales of the half-lives of the radioactive species. In section 5.2, we verified this assumption experimentally.

All the parameters needed for the calculation are also displayed in figure 2. The trap parameters were chosen to correspond to typical operating parameters of the TITAN EBIT. The chosen electron beam energy was twice the threshold energy to completely ionize Mg ions (1.962 keV [17]). Most parameters are well known or easily calculable. However, the radius of the electron beam of the TITAN EBIT is known to be between 150 and 300 μm , when not operated in high compression mode [18]. This range does not sufficiently constrain the calculation of the Spitzer heating rate [7]. This uncertainty was accounted for in the calculation by running the algorithm with different values of electron beam radius inside the range.

Results of the simulation are displayed in figure 4. The total population, defined as the sum of populations of ^{30}Mg , ^{30}Al and ^{30}Si , remained constant until about $t \approx 2.0$ s, when it sharply decreased. According to these results, the newly created ^{30}Al dominates the population after ≈ 300 ms or roughly one $T_{1/2}(^{30}\text{Mg})$, but the population of ^{30}Si could not become dominant before the cloud vanished from the trap ($2 \text{ s} < T_{1/2}(^{30}\text{Al})$).

To understand the contribution of decay energy input to ion losses, the same calculation was performed without any additional recoiling energy. The total storage time was prolonged by only 20%. This indicates that the recoiling energy contributes little to the ion losses in an EBIT when used as storage device, and that losses from Spitzer heating dominate. This finding is in contrast to observations of DRIT in Penning traps [3, 4], where ion losses were attributed to recoil energy exceeding trap barriers.

The results of these simulations were confirmed by an experiment at TITAN facility, which is described in the next section.

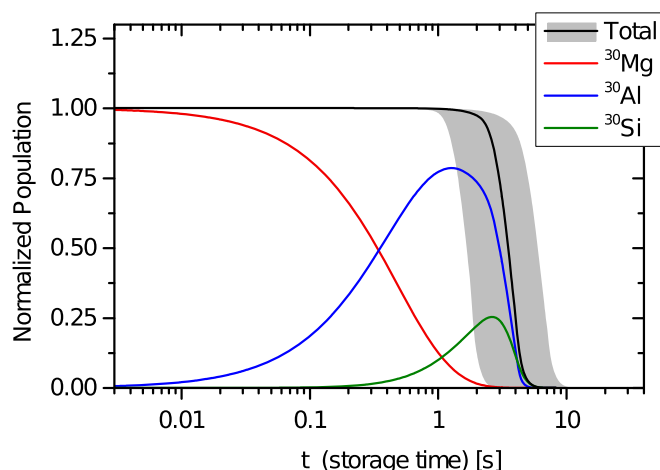


Figure 4. Simulated population evolution of radioactive ions trapped in EBIT. Total population (black curve—normalized to initial) is shown alongside its constituents: ^{30}Mg (red), ^{30}Al (blue) and ^{30}Si (green) populations. The gray band represent the uncertainty of the total population evolution due to electron beam radius.

4. Experiment overview

In the experimental procedure described herein, we investigated RIB population evolution inside the EBIT and tracked ion losses, observed evidence of in-trap decay of radioactive species, and unambiguously identified the daughter species after storage. In addition, we performed an experiment with the secondary beam outside the EBIT to further substantiate the technique.

The experiment was conducted at TRIUMF’s ISOL facility, the isotope separator and accelerator (ISAC) [19]. The RIB was produced by impinging a 480 MeV proton beam onto a uranium-carbide target. Magnesium isotopes were selectively ionized at the target using TRIUMF’s laser ionization source (TRILIS) [20]. The ion beam was extracted, separated by ISAC’s mass separator [21], and sent initially to ISAC’s Yield Station [22] for a composition measurement, which revealed a purity of $\geq 99.4(1)\%$ of $^{30}\text{Mg}^+$.

The $^{30}\text{Mg}^+$ beam was then delivered to TITAN, a multiple-ion-trap system specialized in mass spectrometry and in-trap decay spectroscopy (see figure 5). The beam was accumulated in TITAN’s gas-filled radio-frequency quadrupole cooler and buncher (RFQ) [23], which acts as a preparation trap to deliver cold ion bunches to the other ion traps at TITAN. In this experiment, two were used: the EBIT [24], where DRIT was performed, and the mass measurement penning trap (MPET) [25], where the daughter species was identified in the beam and used in a mass spectrometry experiment.

The TITAN EBIT is designed to provide charge-bred ions for mass measurements with MPET [26] and to perform in-trap decay spectroscopy [27, 28]. In this experiment, the trapping and electron beam parameters were identical to those listed in figure 2. For decay spectroscopy, the EBIT has a large central drift tube with seven viewports, around which photodetectors can be mounted to observe gamma and x-rays emitted from the trapped contents. For mass spectrometry, as beams are extracted from the EBIT and sent towards MPET, they pass through a Bradbury–Nielsen gate (BNG) [29], which selects the bunched beam by its time-of-flight and thus its mass-to-charge ratio (A/q). Additionally, a

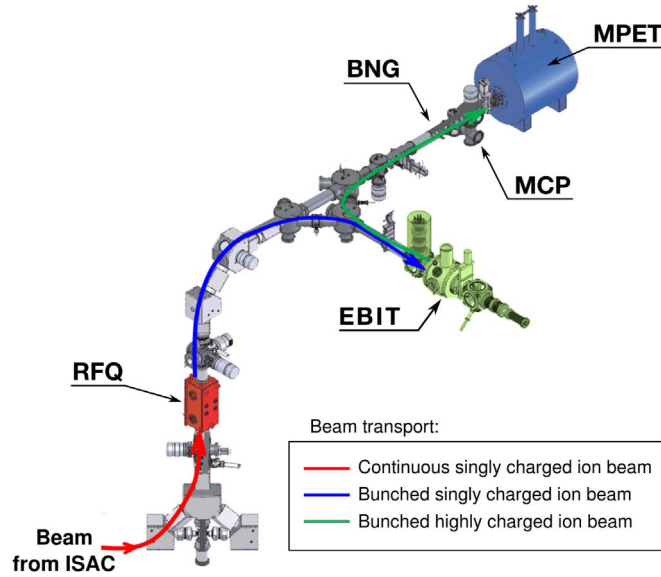


Figure 5. Overview of the TITAN facility highlighting the main components and beam transport path relevant to this experiment. DRIT was performed in EBIT, where the $^{30}\text{Mg}^+$ beam was stored until a population of $^{30}\text{Al}^{+q}$ was formed. The secondary beam was then transported to the MPET for a mass measurement.

microchannel plates detector (MCP) can be moved into the beam line before the MPET. It yields a time-of-flight spectrum that allows the A/q identification of the beam constituents.

The MPET is a precision Penning trap mass spectrometer dedicated to measuring masses of short-lived ion species. It has high resolving power, capable of separating mass differences up to one part in 2 million [25]. The mass (M) of a trapped ion is measured through the measurement of its cyclotron frequency inside a homogeneous magnetic field (of strength B), given by $\nu_c = \frac{q e B}{2\pi M}$, where $q e$ is the charge of the ion.

Our procedure employs the time-of-flight ion cyclotron resonance (ToF-ICR) technique [30] to measure ν_c . The magnetic field B is calibrated by the ν_c measurement of a reference ion of well known mass, typically from a stable ion source or from a stable/residual species present in EBIT's background gas.

5. Population evolution and in-trap decay at TITAN-EBIT

In this section, we describe the systematic study of the evolution of trapped radioactive ion cloud over a range of storage times. To ensure a constant amount of RIB was employed every cycle, the RFQ accumulated ISAC's ^{30}Mg beam for 100 ms. The beam was sent to the EBIT, where the storage time was varied between $t = 15$ ms and 8 s, covering one order of magnitude above and below the half-life of ^{30}Mg . Meanwhile, an HPGe detector monitored the γ -rays from the radioactive decays within the trap volume. After storage, the composition of the ion cloud was inspected by extracting it onto an MCP detector about 10 meters downstream (see figure 5).

The time-of-flight spectrum allowed the identification of the A/q of each species as well as their count rates. Typical time-of-flight spectra can be seen in figure 6 (top panel), where

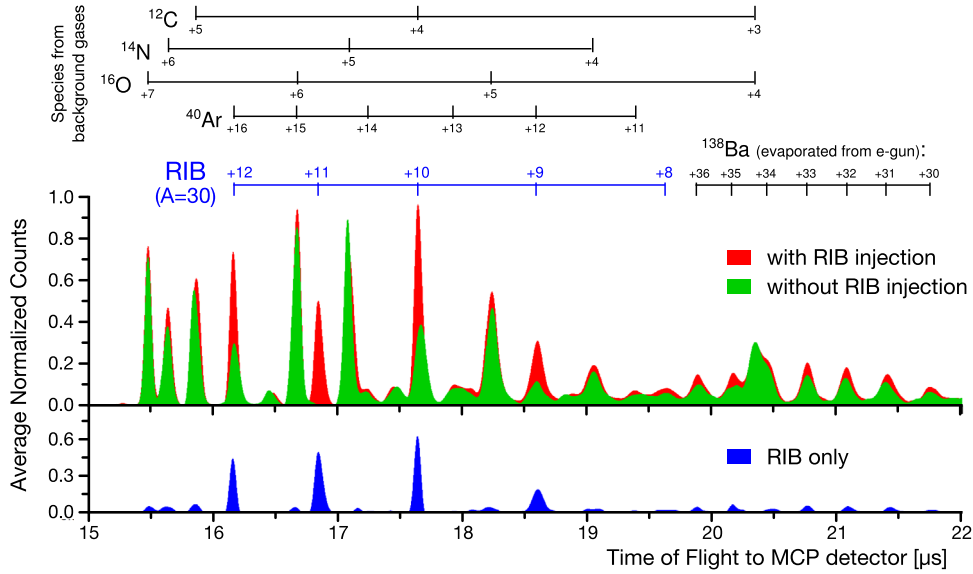


Figure 6. Sample spectra of time-of-flight measurements between EBIT and the MCP (top panel), which allow A/q identification of trapped species. Spectra were obtained with (top, red) and without (top, green) RIB injection into EBIT. RIB peaks can be identified by subtracting the two spectra (bottom, blue). RIB charge states between +9 and +12 of $A = 30$ beam can be clearly identified. Other identified species are also marked for reference.

the average spectra of measurements with $t \geq 100$ ms is shown. As ionized residual gases could have the same A/q as the RIB, spectra were measured with and without the injection of RIB into EBIT under identical conditions. The subtracted spectrum contains only the RIB species and an example can be seen in figure 6 (bottom panel). The spectra obtained at each storage time were analyzed with a multiple-peak fitting routine, through which the count rate for each peak could be determined, including from overlapping peaks.

With the MCP data, we monitored the evolution of both the charge state distribution and the absolute population of RIB. The HPGc detected γ -rays from the decay transitions and provided evidence for the creation of daughter species.

5.1. Achievable storage time

We verified whether the ion cloud could be stored as long as needed to create secondary beams. At each storage time, we analyzed the total count rate of RIB by summing the counts of all RIB peaks present on the spectrum. The result is shown in figure 7.

The total RIB count rate was roughly constant and independent of t up to $t = 2.0$ s, much longer than $T_{1/2}$ (³⁰Mg). This suggests a high re-trapping efficiency of the daughters of ³⁰Mg decay. After $t \approx 2$ s, the RIB count rate dropped. This is shorter than $T_{1/2}$ (³⁰Al), thus the creation of a ³⁰Si beam may not be feasible.

The simulated evolution of the total RIB population (section 3) is overlaid on the data in figure 7 and agrees well with it, with the population loss of $A = 30$ species happening at the same timescale. This result substantiates the simple EBIT thermodynamical model and confirms Spitzer heating as the dominant source of ion losses.

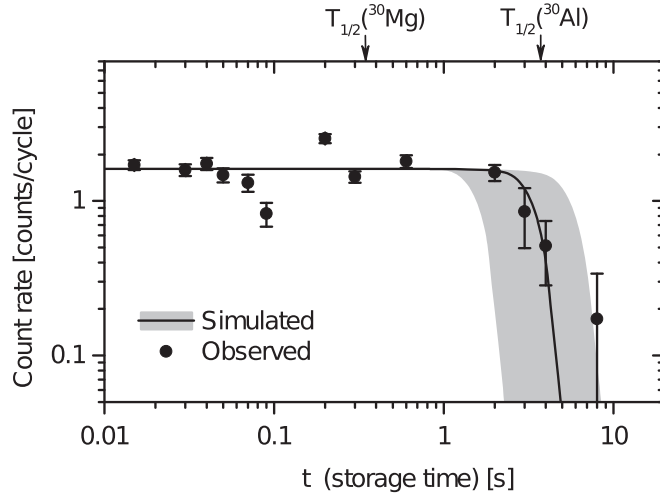


Figure 7. Integrated RIB count rates on the MCP as a function of storage time, obtained from the spectral analysis of time-of-flight data. The simulated RIB population evolution from section 3 is shown normalized to the measured count rate data.

5.2. Charge-state evolution

In EBITs, the storage time governs the charge state distribution of the ion cloud and, thus, it influences confinement and Spitzer heating. It also influences how much background gas gets ionized which may contaminate the secondary beam. Furthermore, if the beam is extracted from EBIT, it needs to match the subsequent device's acceptance. Therefore, the storage time and the desired charge state must be chosen to balance the quality of the secondary beam and the number of daughter species it contains.

To maximize production of secondary beam, optimize its purity, and minimize decay losses for its mass measurement, we analyzed the time-of-flight data looking for charge state evolution of the stored RIB and the presence of contaminants. In figure 6, the RIB peaks corresponding to $q = +9$ to $+12$ can be seen, as well as a series of peaks of background gas species ($^{12}\text{C}^{q+}$, $^{14}\text{N}^{q+}$, $^{16}\text{O}^{q+}$ and $^{40}\text{Ar}^{q+}$) and of $^{138}\text{Ba}^{q+}$, originating from evaporated material from the electron source cathode. In figure 8, the relative populations of each RIB charge state are shown as a function of storage time.

During the storage time interval analyzed, the radioactive trapped ion cloud evolved from charge state $q = +5$ to $+12$. The charge state $q = +11$ dominates the RIB population for $t \gtrsim 300$ ms, which confirms this to be a good charge state to perform the simulations in section 3. It is also clear from figure 6 that the $q = +11$ RIB peak was the most separated charge state from any background species. Thus, it was the best choice to be employed for further study outside of the EBIT.

5.3. γ -ray evidence of in-trap decay

Complementary decay spectroscopy measurements helped to identify the in-trap creation of the daughter species. The γ -rays from the decay of ^{30}Mg and ^{30}Al were detected by a calibrated HPGe detector placed at one of EBIT's optical viewing ports (see figure 1).

A typical γ -ray spectrum is shown in figure 9. Two characteristic transitions in ^{30}Al following the decay of ^{30}Mg were identified (244 and 444 keV), as well as three transitions in

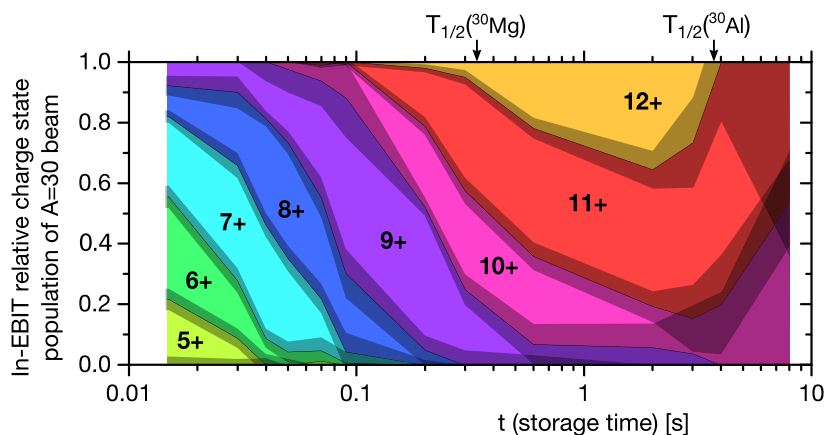


Figure 8. Observed evolution of charge state population of $A = 30$ beam in EBIT as a function of storage time. Relative populations are stacked by charge state. Darkened regions are the error of each population. The increase in uncertainties after 3 s is due to the drop in RIB count rate and to overlap with intense background peaks.

^{30}Si from the ^{30}Al decay (1263, 2235 and 3498 keV). The observed lines are consistent with the known transitions (figure 3(a)).

The measurement cycles also included a background measurement time after the ejection of ions from the EBIT (blue in figure 9). They revealed decay lines of ^{30}Mg and ^{30}Al , which suggests imperfect extraction of ions, but less prominently than when trap was full. A 10 min measurement with ^{30}Mg beam blocked right at the entrance of the TITAN system showed none of the decay lines of ^{30}Mg and ^{30}Al . This reveals that the observed transitions came from locations near or inside the EBIT. A detailed analysis of the obtained γ -ray spectra in this experiment is presented in [31].

6. Identification of daughter species and Penning trap mass spectrometry

Although the systematic measurements performed with EBIT reveal strong evidence of in-trap decay and creation of daughter species, the analysis of the time-of-flight to the MCP cannot distinguish between ^{30}Mg and its daughters. For this reason, the identification of daughter species was performed with the MPET high-precision mass spectrometer, which was followed by a demonstrative experiment using the secondary beam in the same apparatus.

6.1. Identification of daughter species

High-precision mass spectrometry provided unambiguous identification of each species. The relative mass precision required to resolve $^{30}\text{Al}^{+q}$ from $^{30}\text{Mg}^{+q}$ (in the same charge state) is 3×10^{-4} [32], which is well within MPET's capabilities [25].

In the first identification measurement, the RIB was stored in EBIT for $t = 50$ ms, which is much shorter than the half-life of ^{30}Mg (335(10) ms). The BNG selected the +8 charge state of RIB, which was the most populated one (see figure 8). The selected beam was loaded into the MPET, where a search for $^{30}\text{Mg}^{8+}$, $^{30}\text{Al}^{8+}$ and $^{30}\text{Si}^{8+}$ was done. The analysis revealed the presence of $^{30}\text{Mg}^{8+}$, but no detectable amount of $^{30}\text{Al}^{8+}$ or $^{30}\text{Si}^{8+}$ was observed in the beam.

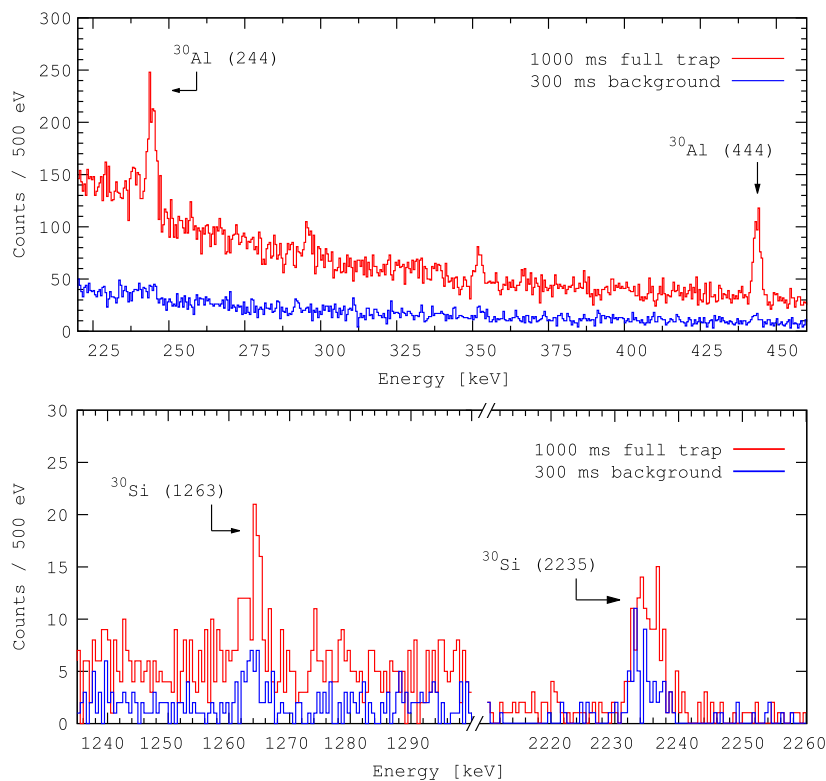


Figure 9. Characteristic decay lines from de-excitation of β -decay daughters ^{30}Al (top) and ^{30}Si (bottom) seen in a typical HPGe γ -ray spectrum. This spectrum was obtained with a storage time of $t = 1000$ ms (red) followed by a 300 ms background measurement after trap was emptied (blue). Background lines of the naturally occurring ^{211}Bi (351.9 keV) and ^{214}Pb (295.5 keV) were also present in the spectra. Adapted from [31].

Likewise, the RIB was stored in EBIT for $t = 300$ ms (close to the half-life of ^{30}Mg), which mostly populated the +11 charge state. This time, $^{30}\text{Al}^{11+}$ was successfully identified in the MPET, confirming the presence of daughter species in the secondary beam. Figure 10 shows a sample ToF-ICR resonance of $^{30}\text{Al}^{11+}$ acquired. Once again, $^{30}\text{Si}^{11+}$ was not observed. However, measurements with a longer storage time in the EBIT, that could enable creation of $^{30}\text{Si}^{11+}$ (see figure 4), were not attempted.

6.2. Demonstrative experiment

The last goal of this proof-of-principle experimental campaign was to use the secondary beam created through DRIT in an experiment outside the storage device. High-precision mass measurements using the MPET are very sensitive to the incoming beam quality. A successful precision mass spectrometry measurement reveals that the beams produced using the technique meet high quality criteria.

High-precision mass measurements of $^{30}\text{Al}^{11+}$ and $^{30}\text{Mg}^{8+}$ were performed; the measurement and analysis procedure followed the same as in [33]. The atomic mass M is calculated through the cyclotron frequency ratio R of the IoI and the reference ion (denoted by

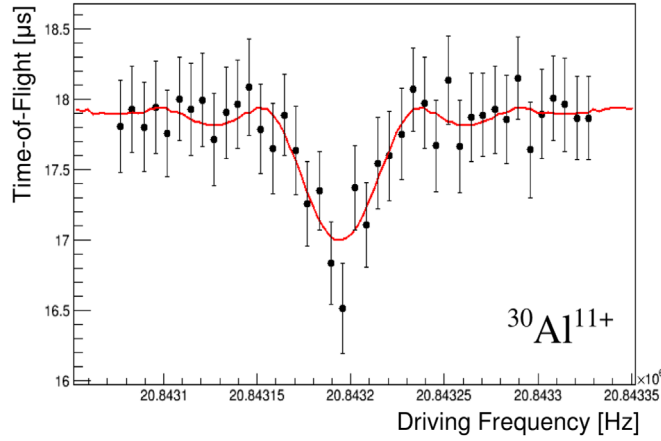


Figure 10. A typical ToF-ICR resonance of $^{30}\text{Al}^{11+}$ measured with MPET. The beam used was created by storing the parent beam for $t = 300$ ms in the EBIT. The red curve is an analytical fit to the data.

Table 1. Atomic masses of ^{30}Al and ^{30}Mg , given as a mass excess. Values presented in this work are compared to [32]. The weighted average of the measured frequency ratios between the IoI and of reference are also given.

IoI	Reference	R	Atomic mass excess (keV)	
			This work	Literature
$^{30}\text{Al}^{11+}$	$^{16}\text{O}^{6+}$	1.022 476 354(95)	−15 863.5 (2.6)	−15 864.8 (2.9)
$^{30}\text{Mg}^{8+}$	$^{39}\text{K}^{10+}$	0.962 122 910(48)	−8 880.9 (1.4)	−8 883.8 (3.4)

subscripts ioi and ref, respectively):

$$R = \frac{\nu_{c,\text{ref}}}{\nu_{c,\text{ioi}}} = \frac{(M_{\text{ioi}} - q_{\text{ioi}} M_e + BE_{\text{ioi}}) q_{\text{ref}}}{(M_{\text{ref}} - q_{\text{ref}} M_e + BE_{\text{ref}}) q_{\text{ioi}}}, \quad (1)$$

where q is the charge state of the ion, M_e is the mass of the electron and BE is the binding energy of all electrons removed from its atomic form. Atomic masses of the reference ions were taken from [32], while electron binding energies were taken from [17].

Results of the mass measurements performed are shown in table 1. Our values agree with the Atomic Mass Evaluation of 2016 [32] and provide a modest improvement on their precision.

7. Conclusions and applications

We successfully demonstrated the DRIT technique using the EBIT at TITAN facility. A cloud of $^{30}\text{Mg}^{q+}$ ions was stored in the EBIT and the creation of a secondary beam containing $^{30}\text{Al}^{q+}$ ions was identified through three signatures: the persistence of the ions in the trap for much longer than the parent's half-life, the observation of γ -rays from the parent's decay, and the identification of $^{30}\text{Al}^{11+}$ through Penning trap mass spectrometry. The extraction for mass measurement in the Penning trap also demonstrate the capability of DRIT to produce beams compatible with subsequent experiments.

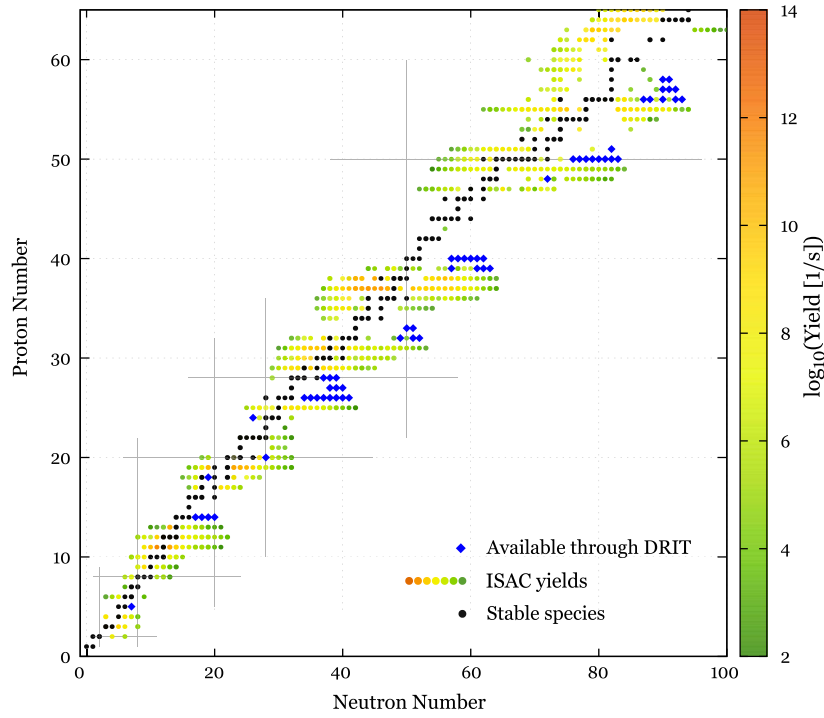


Figure 11. Current yields of radioactive ion beams available at the ISAC facility at TRIUMF [35]. Other species potentially accessible through DRIT are indicated by blue diamonds. These were selected based on the availability of a suitable parent with a minimum yield of 50 pps, maximum half-life of 2 s and $Q_\beta < 15$ MeV.

We performed EBIT simulations to understand losses mechanisms related to re-trapping efficiency. Simulated results agree with the observations made in the experiment and indicate that Spitzer heating is the main source of observed losses, and not the recoil energy from β -decay. Our results are in line with findings of other experiments performed using DRIT with EBITs as storage media [5, 6], which indicated high re-trapping efficiency of decay products. However, they contrast with those performed in Penning traps [3, 4], which suggest a large influence of the recoil energy in the observed efficiencies.

EBITs are reliable storage devices for DRIT. They have demonstrated superior confinement capabilities, higher charge-space limit, and larger recapture efficiencies than other ion traps. Moreover, Spitzer heating depends on operating parameters that can be tuned for specific experiments. Since EBITs are regularly employed in RIB facilities to provide charge-bred beams for experiments and post-acceleration, this technique has potential to become a regular tool to increase beam availability.

DRIT can allow access to non-ISOL beams at ISOL facilities. For example, ^{34}Si , a nuclide that was object of special interest in recent years [34], could be produced from ^{34}Al . At ISAC facility, over 50 new species are potentially accessible through DRIT. These are shown in figure 11 together with the currently available RIB yields [35]. They were identified based on the availability of a suitable parent with a minimum yield of 50 pps, $Q_\beta < 15$ MeV and, in accordance with the results of this experiment, maximum half-life of 2 s. As can be seen, beams of typical non-ISOL RIBs are within reach, such as of B, Si, Fe and Zr neutron-

rich isotopes. Many more species would be available upon the increase of the maximum half-life constraint.

The technique can also give direct access to certain nuclear isomers, in some cases devoid of contamination from the ground state. For example, the long-lived isomeric 1^+ state of ^{34}Al , for instance, has been an object of curiosity [36–38] and is preferentially and cleanly populated only through a ^{34}Mg parent beam. Another remarkable example is the production of the $^{229\text{m}}\text{Th}$ ‘nuclear clock’ isomer [39–41], which is typically generated by a 2% decay branch in the ^{233}U α -decay. An alternative route of production is through the 13.4% branch in the β -decay of ^{229}Ac , available in high intensities at ISOL facilities. If $^{229\text{m}}\text{Th}$ daughters are recaptured in an EBIT, the charge breeding immediately promotes the suppression of internal conversion, its dominant decay branch [41].

In some cases, better beam properties could be achieved through DRIT even for available beams. Despite the probably lower yields, potential gains in purity may make the production from a parent beam more advantageous than the direct production of the desired species. An example is the measurement of the Q -value of the superallowed β decay $^{74}\text{Rb} \rightarrow ^{74}\text{Kr}$ [26, 42]. Noble gases produced in ISOL facilities suffer from high levels of contamination co-produced in the ion sources. In contrast, pure alkali beams are commonly available. A ^{74}Kr beam can be more cleanly produced through the decay of ^{74}Rb .

Acknowledgments

The authors want to thank Oliver Kester and Friedhelm Ames for the valuable discussions and the TRILIS group and TRIUMF staff for their support in beam delivery. This work was partially supported by Natural Sciences and Engineering Research Council of Canada (NSERC), the Canada Foundation for Innovation (CFI), the Brazilian Conselho Nacional de Desenvolvimento Científico e Tecnológico (CNPq) (grant 249121/2013-1), and the Deutsche Forschungsgemeinschaft (DFG) (grant FR 601/3-1).

ORCID iDs

E Leistenschneider  <https://orcid.org/0000-0003-0377-8523>

References

- [1] Blumenfeld Y, Nilsson T and Van Duppen P 2013 Facilities and methods for radioactive ion beam production *Phys. Scr.* **2013** 14023
- [2] Gottberg A 2016 Target materials for exotic ISOL beams *Nucl. Instrum. Methods Phys. Res. B* **376** 8–15
- [3] Herlert A *et al* 2005 Mass spectrometry of atomic ions produced by in-trap decay of short-lived nuclides *New J. Phys.* **7** 44
- [4] Herlert A *et al* 2012 Recoil-ion trapping for precision mass measurements *Eur. Phys. J. A* **48** 97
- [5] de Walle J *et al* 2009 In-trap decay of ^{61}Mn and Coulomb excitation of $^{61}\text{Mn}/^{61}\text{Fe}$ *Eur. Phys. J. A* **42** 401
- [6] Gaffney L P *et al* 2015 Low-energy Coulomb excitation of ^{62}Fe and ^{62}Mn following in-beam decay of ^{62}Mn *Eur. Phys. J. A* **51** 136
- [7] Currell F and Fussmann G 2005 Physics of electron beam ion traps and sources *IEEE Trans. Plasma Sci.* **33** 1763–77
- [8] Zschornacka G, Schmidt M and Thorn A 2014 Electron beam ion sources. Contribution to the CAS-CERN Accelerator School: Ion Sources, Senec, Slovakia, 29 May–8 June 2012 *CERN Yellow Report CERN-2013-00* CERN (<https://doi.org/10.5170/CERN-2013-007.165>)

- [9] Dilling J *et al* 2006 Mass measurements on highly charged radioactive ions, a new approach to high precision with TITAN *Int. J. Mass Spectrom.* **251** 198–203
- [10] Wenander F 2010 Charge breeding of radioactive ions with EBIS and EBIT *J. Instrum.* **5** C10004
- [11] Frekers D *et al* 2013 Penning-trap Q-value determination of the $^{71}\text{Ga}(\nu, e)^{71}\text{Ge}$ reaction using threshold charge breeding of on-line produced isotopes *Phys. Lett. B* **722** 233–7
- [12] Olaizola B *et al* 2016 High-sensitivity study of levels in ^{30}Al following β decay of ^{30}Mg *Phys. Rev. C* **94** 054318
- [13] Alburger D E and Goosman D R 1974 Decay schemes of ^{30}Al , ^{30}P , and ^{20}O *Phys. Rev. C* **9** 2236–42
- [14] ENSDF (Evaluated Nuclear Structure Data File) 2018 National Nuclear Data Center On-Line Data Service, ENSDF database (Accessed: 20 August 2018) www.nndc.bnl.gov/ensdf/
- [15] Kozlov V Y 2004 Physics and present status of the WITCH experiment *Phys. At. Nucl.* **67** 1112–8
- [16] Coeck S 2007 Search for non standard model physics in nuclear beta-decay with the WITCH experiment *PhD Thesis* Leuven U
- [17] Rodrigues G C, Indelicato P, Santos J P, Patté P and Parente F 2004 Systematic calculation of total atomic energies of ground state configurations *At. Data Nucl. Data Tables* **86** 117–233
- [18] Froese M W 2006 The TITAN electron beam ion trap: assembly, characterization, and first tests *Master's Thesis* University of Manitoba
- [19] Ball G C, Hackman G and Krücken R 2016 The TRIUMF-ISAC facility: two decades of discovery with rare isotope beams *Phys. Scr.* **91** 93002
- [20] Lassen J, Bricault P, Dombisky M, Lavoie J P, Gillner M, Gottwald T, Hellbusch F, Teigelhöfer A, Voss A and Wendt K D A 2009 Laser ion source operation at the TRIUMF radioactive ion beam facility *AIP Conf. Proc.* **1104** 9–15
- [21] Bricault P, Baartman R, Dombisky M, Hurst A, Mark C, Stanford G and P Schmor 2002 TRIUMF-ISAC target station and mass separator commissioning *Nucl. Phys. A* **701** 49–53
- [22] Kunz P, Andreoiu C, Bricault P, Dombisky M, Lassen J, Teigelhöfer A, Heggen H and Wong F 2014 Nuclear and in-source laser spectroscopy with the ISAC yield station *Rev. Sci. Instrum.* **85** 53305
- [23] Brunner T *et al* 2012 TITAN's digital RFQ ion beam cooler and buncher, operation and performance *Nucl. Instrum. Methods Phys. Res. A* **676** 32–43
- [24] Lapierre A *et al* 2010 The TITAN EBIT charge breeder for mass measurements on highly charged short-lived isotopes—first online operation *Nucl. Instrum. Methods Phys. Res. A* **624** 54–64
- [25] Brodeur M *et al* 2012 Verifying the accuracy of the TITAN Penning-trap mass spectrometer *Int. J. Mass Spectrom.* **310** 20–31
- [26] Ettenauer S *et al* 2011 First use of high charge states for mass measurements of short-lived nuclides in a Penning trap *Phys. Rev. Lett.* **107** 272501
- [27] Lennarz A *et al* 2014 In-trap spectroscopy of charge-bred radioactive ions *Phys. Rev. Lett.* **113** 082502
- [28] Leach K G *et al* 2015 The TITAN in-trap decay spectroscopy facility at TRIUMF *Nucl. Instrum. Methods Phys. Res. A* **780** 91–9
- [29] Brunner T *et al* 2012 A large Bradbury Nielsen ion gate with flexible wire spacing based on photo-etched stainless steel grids and its characterization applying symmetric and asymmetric potentials *Int. J. Mass Spectrom.* **309** 97–103
- [30] König M, Bollen G, Kluge H-J, Otto T and Szerypo J 1995 Quadrupole excitation of stored ion motion at the true cyclotron frequency *Int. J. Mass Spectrom. Ion Process* **142** 95–116
- [31] Lennarz A 2015 In-trap decay spectroscopy on highly-charged radioactive ions towards measurements on intermediate nuclei in $\beta\beta$ *PhD Thesis* Westfälischen Wilhelms-Universität Münster
- [32] Huang W J, Audi G, Wang M, Kondev F G, Naimi S and Xu X 2017 The AME2016 atomic mass evaluation (I). Evaluation of input data; and adjustment procedures *Chin. Phys. C* **41** 030002
- [33] Lascar D *et al* 2017 Precision mass measurements of $^{125\sim 127}\text{Cd}$ isotopes and isomers approaching the $n = 82$ closed shell *Phys. Rev. C* **96** 044323
- [34] Mutschler A *et al* 2017 A proton density bubble in the doubly magic ^{34}Si nucleus *Nat. Phys.* **13** 152–6
- [35] TRIUMF 2018 ISAC Yield Database (Accessed: 23 August 2018) <http://isys01.triumf.ca/search/yield/data>
- [36] Kwiatkowski A A *et al* 2015 Observation of a crossover of S_{2n} in the island of inversion from precision mass spectrometry *Phys. Rev. C* **92** 061301

- [37] Lica R *et al* 2017 Identification of the crossing point at $n = 21$ between normal and intruder configurations *Phys. Rev. C* **95** 021301
- [38] Rotaru F *et al* 2012 Unveiling the intruder deformed 0_2^+ state in ^{34}Si *Phys. Rev. Lett.* **109** 092503
- [39] von der Wense L *et al* 2016 Direct detection of the ^{229}Th nuclear clock transition *Nature* **533** 47–51
- [40] von der Wense L, Seiferle B and Thirof P G 2018 Towards a ^{229}Th -based nuclear clock *Meas. Tech.* **60** 1178–92
- [41] Seiferle B, von der Wense L and Thirof P G 2017 Lifetime measurement of the ^{229}Th nuclear isomer *Phys. Rev. Lett.* **118** 042501
- [42] Malbrunot-Ettenauer S *et al* 2015 Penning trap mass measurements utilizing highly charged ions as a path to benchmark isospin-symmetry breaking corrections in ^{74}Rb *Phys. Rev. C* **91** 045504